Phase Noise Integration Limits for Jitter Calculation

Yu Zhao
Electrical and Computer Engineering Department
University of California, Los Angeles, CA 90095, USA
zhaoyu@ucla.edu

Behzad Razavi
Electrical and Computer Engineering Department
University of California, Los Angeles, CA 90095, USA
razavi@ee.ucla.edu

***Abstract*—High-speed wireline transceivers and analog-to-digital converters are sensitive to broadband phase noise of their clocks. It is generally assumed that the total rms jitter can be computed by integration of the phase noise profile up to the Nyquist rate. This paper shows that the integration limits depend on the measurement or simulation environment and, in some cases, must be chosen equal to twice the Nyquist rate.**

I. INTRODUCTION

The problem of jitter has assumed new dimensions as communication systems seek higher date rates. In wireline transmitters, for example, the entire phase noise profile of the clock applied to the last multiplexing stage translates to output jitter. Similarly, the broadband jitter of the clock(s) driving high-speed interleaved analog-to-digital converters (ADCs) (e.g., in a wireline receiver) corrupts the sampled signals. For this reason, the phase noise must be integrated up to high frequency offsets [1–3]. A common assumption is that the integration up to an offset equal to half of the clock frequency (the "Nyquist rate") yields the total jitter [4, 5], but we show here that this is not always correct.

This paper provides an analytical foundation to answer two key questions. (1) Up to what offset frequency must the phase noise be integrated? We prove that the limit depends on the situation. (2) Should the phase noise around the higher harmonics of the clock be included? We offer a perspective that obviates the need for dealing with harmonics.

Section II is concerned with phase noise aliasing. Section III and Section IV describe how the phase noise must be integrated in circuit simulations and experimental measurements, respectively. Section V presents simulation results supporting the analyses.

II. PHASE NOISE ALIASING

Consider a sinusoidal waveform containing a random continuous-time phase fluctuation, $x(t) = A\cos[2\pi f_{CK}t + \phi_n(t)]$. We exclude deterministic spurs here. The phase noise spectrum, $S_{\phi_n}(f)$, is centered around the zero frequency and, in a phase-locked environment, exhibits a plateau and a long tail [Fig. 1(a)]. We apply this signal to two noiseless inverters so as to obtain approximately a square wave. Each value of $\phi_n(t)$ around the zero crossings of $x(t)$ translates to a random edge displacement in this output, denoted by $\Delta\phi_1$, $\Delta\phi_2$, etc. We wish to compute the spectrum of these displacement and find their rms value. Assuming $|\Delta\phi_j| \ll 1$ rad, we can view these quantities as discrete-time samples of $\phi_n(t)$; that is

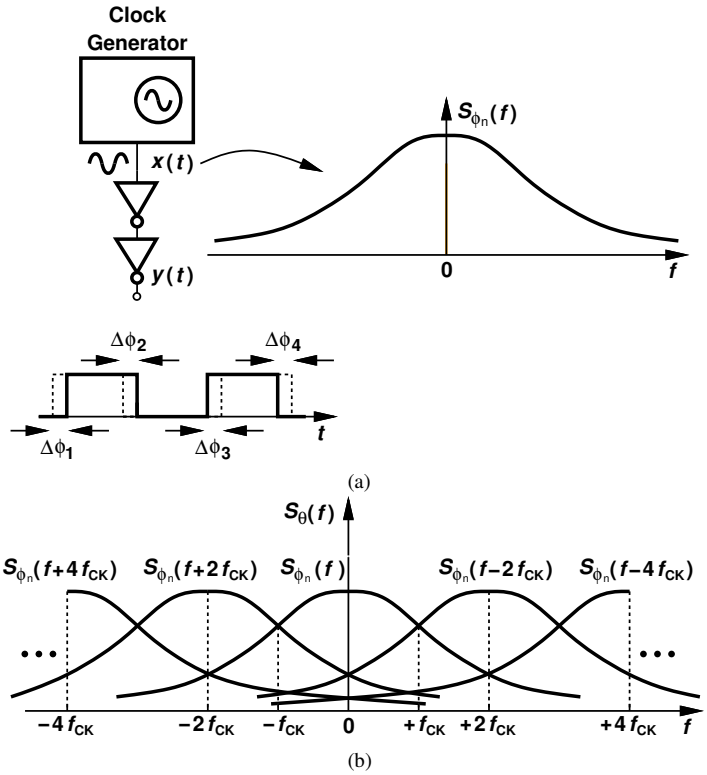

Fig. 1. (a) Noisy sine and its phase spectrum, and (b) spectrum of square wave jitter.

$$\Delta\phi_j = \phi_n(t - j\frac{T_{CK}}{2})\delta(t - j\frac{T_{CK}}{2}), \tag{1}$$

where j is an integer number and $T_{CK} = 1/f_{CK}$. We denote this discrete-time signal by $\theta(t)$ and its spectrum by $S_\theta(f)$. To obtain $S_\theta(f)$, we shift the spectrum of $\phi_n(t)$ to the left and to the right by integer multiples of $2f_{CK}$ [Fig. 1(b)]. It follows that

$$S_\theta(f) = \sum_{j=-\infty}^{+\infty} S_{\phi_n}(f - 2jf_{CK}). \tag{2}$$

We should make two remarks. First, any attempt to *measure* the zero-crossing phase errors of the sinusoidal waveform, $x(t)$, in Fig. 1(a) would inevitably sample $\phi_n(t)$ and lead to aliasing as well. Second, while it is intuitively meaningful to define "jitter" for $y(t)$ as $\Delta\phi_j$, it is less so for $x(t)$. We must then determine exactly what the area under $S_{\phi_n}(f)$ represents.

978-1-6654-8485-5/22/$31.00 ©2022 IEEE

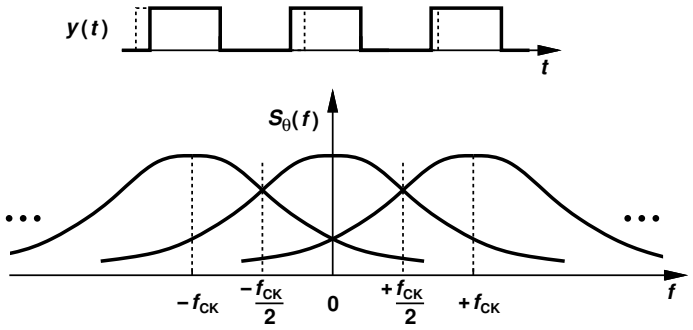

Fig. 2. Jitter measurement sensing only the rising edges of $y(t)$ and corresponding phase noise spectrum.

In the next step, we calculate the rms value of $\Delta\phi_j$ in Fig. 1(a). Parseval's theorem for discrete-time signals tells us that, for a sampling-rate of f_s, this is obtained by integrating the spectrum from $-f_s/2$ to $+f_s/2$. In Fig. 1(b), therefore, we must integrate $S_\theta(f)$ from $-f_{CK}$ to $+f_{CK}$. We observe that $S_\theta(f)$ over this range contains both the contribution of the original spectrum, $S_{\phi_n}(f)$, and the folded tails of $S_{\phi_n}(f \pm 2f_{CK})$, $S_{\phi_n}(f \pm 4f_{CK})$, etc. The tail contribution of $S_{\phi_n}(f \pm 2f_{CK})$ to the range of $[-f_{CK} \ + f_{CK}]$ is equivalent to the noise of $S_{\phi_n}(f)$ in the range of $[-3f_{CK} \ - f_{CK}]$ and $[+f_{CK} \ + 3f_{CK}]$. The same point applies to the tails of the other replicas, yielding

$$\int_{-f_{CK}}^{+f_{CK}} S_\theta(f)df = \int_{-\infty}^{+\infty} S_{\phi_n}(f)df. \tag{3}$$

This relation proves that the rms jitter of the square wave, $y(t)$, in Fig. 1(a) can be obtained by integrating the spectrum of $\phi_n(t)$ from $-\infty$ to $+\infty$ and taking the square root of the result:

$$\sigma_{jit,y(t)} = \frac{1}{2\pi f_{CK}} \sqrt{\int_{-\infty}^{+\infty} S_{\phi_n}(f)df}. \tag{4}$$

We now make two important observations. First, the foregoing analysis deals with only the spectra of the *phase* quantities rather than with the spectra of $x(t)$ and $y(t)$ in Fig. 1(a). Thus, the results are independent of the harmonic contents of these waveforms, obviating the need for considering the phase noise around the harmonics of the clock frequency. For phase noise measurements on a spectrum analyzer, however, the situation is different (Section IV).

Second, if the act of jitter measurement senses the phase errors on both rising and falling edges of a waveform and produces the corresponding spectrum, then this spectrum must be integrated from $-f_{CK}$ to $+f_{CK}$. This point stands in contrast to the typical assumption that the jitter can be obtained by integrating up to the Nyquist frequency, $\pm f_{CK}/2$. On the other hand, if jitter measurement senses only the rising (or falling) edges and constructs the spectrum accordingly (Fig. 2), then the integration must span the first Nyquist zone, $[-f_{CK}/2 + f_{CK}/2]$. These two types of measurements deliver the same rms jitter but should not be confused with each other.

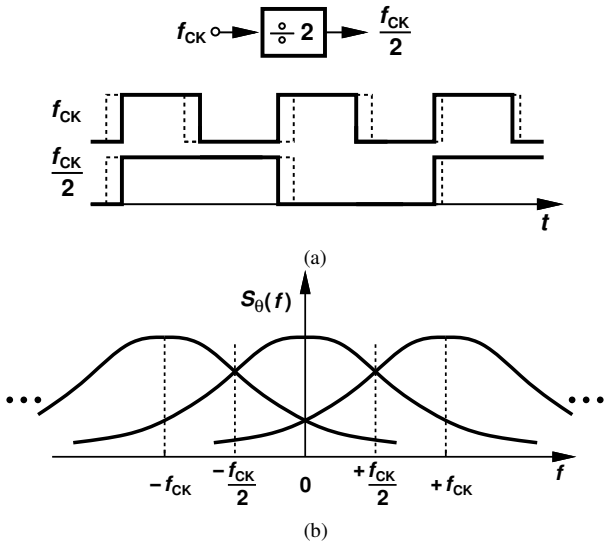

Fig. 3. (a) Output of a $\div 2$ circuit with jittery input, (b) output phase noise profile if both rising and falling edges are considered.

The practical significance of this point becomes clearer in Sections III and IV.

From the above analysis, we can also determine how the phase noise must be integrated at the output of frequency dividers or multipliers. Consider, for example, the $\div 2$ stage shown in Fig. 3(a). If the measurement mechanism senses the random phase departures of both the rising and falling edges of the output, then the integration must extend to $\pm f_{CK}/2$. However, if only the rising or falling edges are considered, the integration occurs up to the Nyquist rate, $\pm f_{CK}/4$.

III. Integration Limits in Circuit Simulations

The question of phase noise integration limits also arises in design and simulations. To compute the jitter of a phase-locked clock, one can perform periodic steady state (pss) and periodic noise (pnoise) simulations in Cadence and obtain the phase noise profile. But the integration limits depend on the exact method of analysis. (1) If Cadence's "time average" method is used, the phase noise plot generated by Cadence must be integrated from $-f_{CK}$ to $+f_{CK}$ because this routine senses both rising and falling edges. (2) If the "jitter" method is used, then Cadence can be instructed to sense only the rising or falling edges. The integration limits of the resulting profile are therefore equal to $\pm f_{CK}/2$.

Another method of jitter simulation is based on the transient noise analysis in Cadence, wherein noise components within a specified frequency range are injected into time-domain waveforms. To compute the rms jitter, one can measure the edge displacements. This is more readily accomplished as depicted in Fig. 4, where a noiseless reference with the same frequency and nominal phase is also generated, and the "delay" function in Cadence's calculator is used to obtain $\Delta\phi_1$, $\Delta\phi_2$, etc. This simulation, however, takes longer, especially for complex circuits, than pss and pnoise analyses.

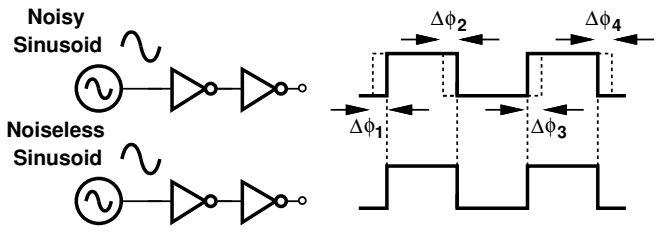

Fig. 4. Transient noise simulation test bench.

An alternative transient noise technique is to determine the spectrum of the entire waveform of interest, an approach that is similar to spectrum analyzer measurements and is described in the next section.

IV. Integration Limits in Experimental Measurements

The phase noise of periodic waveforms can be measured by phase noise analyzers, but only up to an offset frequency of a few hundred megahertz. For example, Keysight's E5052B signal analyzer computes the phase noise for a maximum offset of 100 MHz. For broadband jitter characterization, on the other hand, we must resort to direct reading of the phase noise on a spectrum analyzer. This task poses additional issues.

Suppose the square wave, $y(t)$, in Fig. 5(a) is applied to a spectrum analyzer. We now face the spectrum of a voltage (or current) rather than that of the phase. The spectrum displayed by the analyzer is derived as follows. We approximate the jittery square wave, $y(t)$, by an ideal component, $p(t)$, plus narrow pulses occurring around the transitions, $q(t)$ [Fig. 5(a)]

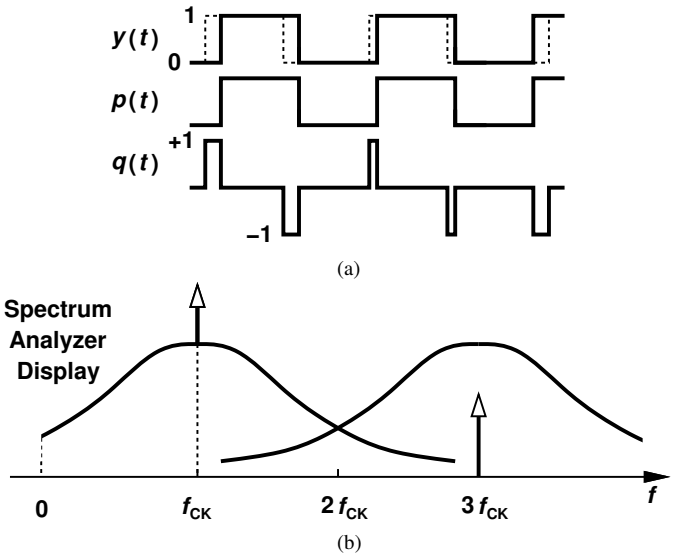

Fig. 5. (a) Square wave with jitter on rising and falling edges and, (b) spectrum analyzer display.

[6]. The latter can be approximated by two trains of impulses:

$$q(t) = \sum_{j=-\infty}^{+\infty} \phi_n(t)\delta(t - jT_{CK}) - \sum_{j=-\infty}^{+\infty} \phi_n(t)\delta(t - jT_{CK} - T_{CK}/2). \quad (5)$$

Note that $q(t)$ is a voltage quantity, but, with the unity amplitude assumed for $y(t)$, the weights of the impulses are equal to samples of $\phi_n(t)$. It can be shown that the spectrum of $q(t)$ contains replicas at only the odd harmonics of the clock frequency:

$$S_q(f) = \sum_{j=-\infty}^{+\infty} S_{\phi_n}\left[f - (2j+1)f_{CK}\right]. \quad (6)$$

The analyzer's display thus emerges as depicted in Fig. 5(b), where the declining impulses represent the ideal square wave, and the replicas expressed by Eq. (6) appear with *equal* heights. The key point here is that phase noise integration must begin from $f = f_{CK}$ and extend to a frequency offset equal to f_{CK} ($f = 2f_{CK}$). Thus, integration up to the Nyquist rate underestimates the jitter here as well.

V. Simulation Results

A number of simulations have been performed in Cadence to verify the calculations in the previous sections. In order to create a jittery sinusoid, we (a) apply white noise to a first-order low-pass filter having a bandwidth of f_1, and (b) use the approximation $x(t) = A\cos[2\pi f_{CK}t + \phi_n(t)] \approx A\cos(2\pi f_{CK}t) - A\sin(2\pi f_{CK}t)\phi_n(t)$ to generate $x(t)$. (This approximation generates negligible AM noise.) We select f_{CK} = 10 GHz and f_1 = 10 MHz, 100 MHz, or 1 GHz. The spectrum of $\phi_n(t)$ is shown in Fig. 6(a).

Next, we examine the phase noise at the output of the inverters in Fig. 1(a), and plot it in Fig. 6(b). The aliasing from higher replicas is observed. Applying this waveform to a noiseless ÷2 stage yields the plots depicted in Fig. 6(c). We can now integrate these profiles according to our findings and determine the validity of our derivations. Table I summarizes the integration bandwidths and corresponding rms jitter values.

In order to emulate the spectrum analyzer operation described in Section IV, we run a transient noise analysis and compute the power spectral density (PSD) of $y(t)$ in Fig. 1(a). Plotted in Fig. 7, the result confirms that the replicas of $S_{\phi_n}(f)$ exhibit the same height. The plateaus around 10 GHz and 30 GHz are not visible at this scale, but the noise at high offsets

TABLE I. Simulation Results

f_1 (Hz)	Theoretical Jitter Values (fs)	Simulated Jitter Values (fs)	
		w/o div	w/ div
10 M	28.21	28.34	28.34
100 M	89.21	89.51	89.61
1 G	282.1	280.5	282.6

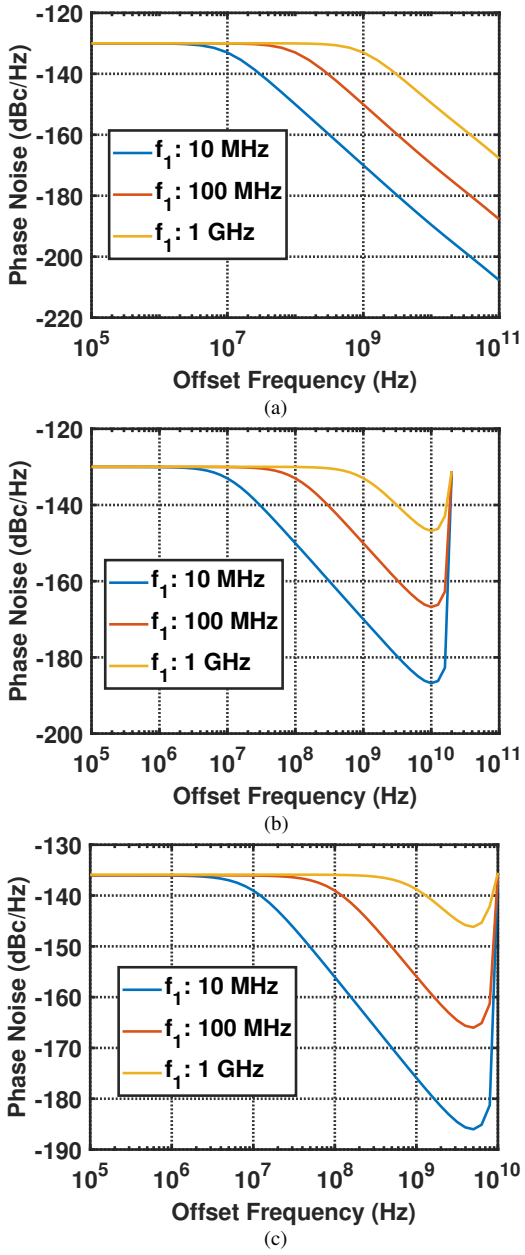

Fig. 6. Simulated spectrum of (a) $\phi_n(t)$, (b) $\theta(t)$ and, (b) $\div 2$ output phase noise.

follows the behavior depicted in Fig. 6(a) for different values of f_1. Integration of these profiles from $f = 0$ to $f = 20$ GHz (i.e. up to an offset equal to twice the Nyquist rate) yields rms jitter values equal 29.3 fs, 91.8 fs, and 287.6 fs for $f_1 = 10$ MHz, 100 MHz, and 1 GHz, respectively. (The peaks in the spectrum at DC and 10 GHz are removed from integration.) These results closely agree with those in Table I.

VI. Conclusion

This paper provides a rigorous analysis and prescribes proper phase noise integration limits in various cases. It is shown that integration up to the Nyquist rate is valid only in some cases. In others, the limit must reach twice this value.

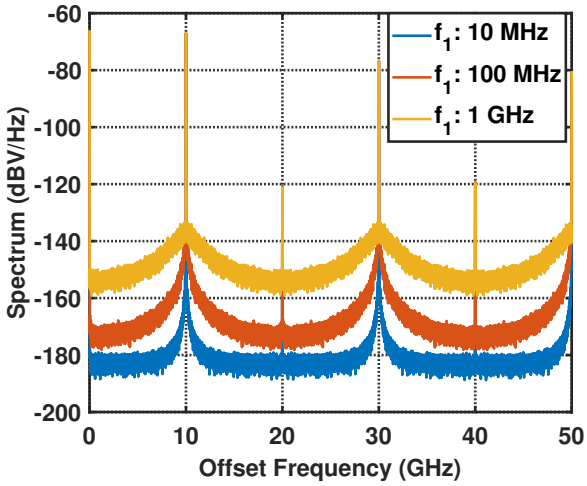

Fig. 7. Power spectral density of $y(t)$ from transient noise simulations.

Acknowledgments

This research is supported by Realtek Semiconductor.

References

[1] M.-S. Chen, Y.-N. Shih, C.-L. Lin, H.-W. Hung, and J. Lee, "A Fully-Integrated 40-Gb/s Transceiver in 65-nm CMOS Technology," *IEEE J. Solid-State Circuits*, vol. 47, no. 3, pp. 627–640, 2012.

[2] R. Navid *et al.*, "A 40 Gb/s Serial Link Transceiver in 28 nm CMOS Technology," *IEEE J. Solid-State Circuits*, vol. 50, no. 4, pp. 814–827, 2015.

[3] T. Ali *et al.*, "A 180mW 56Gb/s DSP-Based Transceiver for High Density IOs in Data Center Switches in 7nm FinFET Technology," in *IEEE ISSCC Dig. Tech. Papers*, 2019, pp. 118–120.

[4] Y. Chang, A. Manian, L. Kong, and B. Razavi, "An 80-Gb/s 44-mW Wireline PAM4 Transmitter," *IEEE J. Solid-State Circuits*, vol. 53, no. 8, pp. 2214–2226, 2018.

[5] E. Depaoli *et al.*, "A 64 Gb/s Low-Power Transceiver for Short-Reach PAM-4 Electrical Links in 28-nm FDSOI CMOS," *IEEE J. Solid-State Circuits*, vol. 54, no. 1, pp. 6–17, 2019.

[6] A. Homayoun and B. Razavi, "Analysis of Phase Noise in Phase/Frequency Detectors," *IEEE Transactions on Circuits and Systems I: Regular Papers*, vol. 60, no. 3, pp. 529–539, 2013.